THE JOURNAL OF PHYSICAL CHEMISTRY Letters

Letter

Cite This: J. Phys. Chem. Lett. 2018, 9, 2196−2201

pubs.acs.org/JPCL

Critical Role of Water in Defect Aggregation and Chemical Degradation of Perovskite Solar Cells

Yun-Hyok Kye,[†] Chol-Jun Yu,*[,†] Un-Gi Jong,[†] Yue Chen,[‡] and Aron Walsh*[,¶]

[†]Computational Materials Design (CMD), Faculty of Materials Science, Kim Il Sung University, Ryongnam-Dong, Taesong District, Pyongyang, Democratic People's Republic of Korea

[‡]Department of Mechanical Engineering, The University of Hong Kong, Pokfulam Road, Hong Kong SAR, China

[¶]Department of Materials, Imperial College London, London SW7 2AZ, United Kingdom

Supporting Information

ABSTRACT: The chemical stability of methylammonium lead iodide ($MAPbI_3$) under humid conditions remains the primary challenge facing halide perovskite solar cells. We investigate defect processes in the water-intercalated iodide perovskite ($MAPbI_3$_H_2O) and monohydrated phase ($MAPbI_3{\cdot}H_2O$) within a first-principles thermodynamic framework. We consider the formation energies of isolated and aggregated vacancy defects with different charge states under I-rich and I-poor conditions. It is found that a PbI_2 (partial Schottky) vacancy complex can be formed readily, while the MAI vacancy complex is difficult to form in the hydrous compounds. Vacancies in the hydrous phases create deep charge transition levels, indicating the degradation of the lead halide perovskite upon exposure to moisture. Electronic structure analysis supports a mechanism of water-mediated vacancy pair formation.

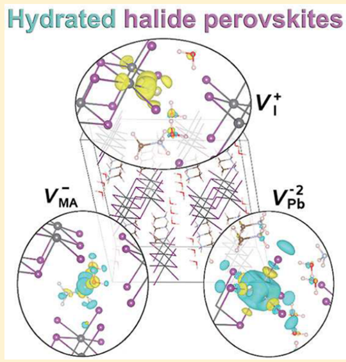

Low-cost perovskite solar cells (PSCs) based on methylammonium lead iodide ($CH_3NH_3PbI_3$ or $MAPbI_3$) are rapidly evolving, with a record power conversion efficiency (PCE) from under 4% in 2009[1] to over 22% in recent years.[2] However, PSCs have a critical problem of easy degradation by extrinsic as well as intrinsic factors, still preventing their outdoor installation.[3−5] In particular, the facile decomposition of $MAPbI_3$ upon exposure to moisture has been recognized to be the major extrinsic factor of PSC degradation.[6−8] In fact, the PCE of $MAPbI_3$ solar cells drops by nearly 90% in a few days under an ambient environment (T = 300 K, relative humidity (RH) = 30−50%),[9] while $MAPbI_3$ can be decomposed into MAI, PbI_2, and HI in a few hours at high humidity conditions.[10]

For a chemical explanation of this phenomenon, hydrolysis of $MAPbI_3$ was initially suggested as the main mechanism, and based on the first-principles calculations, deprotonation of MA^+ by H_2O was proposed as the principal cause of the hydrolysis.[11−13] Soon afterward, however, it was demonstrated that $MAPbI_3$ readily transformed to the monohydrate phase $MAPbI_3{\cdot}H_2O$ at moderate humidity (RH ≤ 60%), while it transitioned to the dihydrate phase $(MA)_4PbI_6{\cdot}2H_2O$ at high humidity (RH ≥ 80%), at the initial stage of the $MAPbI_3$ water-mediated decomposition process, which could be reversed by drying treatment.[14−21] This can be explained by the hydrogen bonding interaction between the lead iodide framework and the organic MA^+ cations in the perovskite crystal being weakened upon its hydration.[22−24] MA^+ can readily diffuse and separate from the PbI_6 octahedra, resulting in rapid decomposition of $MAPbI_3$. The activation barrier for vacancy-mediated MA^+ migration was confirmed to be reduced from 1.18 eV in $MAPbI_3$ to 0.38 eV in water-intercalated and 1.14 eV in monohydrated phases.[25−28] Although there have been some theoretical studies of the intrinsic point defects in $MAPbX_3$ (X = I, Br, Cl),[29−33] those in the hydrate phases remain unexplored.

In this Letter, we investigate the origin of perovskite decomposition through point defect processes in water-intercalated $MAPbI_3$, denoted as $MAPbI_3$_H_2O hereafter, and the monohydrated phase, $MAPbI_3{\cdot}H_2O$. Water-intercalated $MAPbI_3$_H_2O is suggested as an intermediate phase during the transition to the hydrated phases due to the relatively low activation energies for water insertion into the perovskite surface (0.27[34] or 0.31 eV[35]), as well as for water molecular diffusion within the bulk crystal (0.28 eV[28]). A density functional theory (DFT) approach combined with ab initio thermodynamics is utilized to describe defect formation and interactions. Electrostatic stabilization by water is found to play a key role in defect clustering and, ultimately, in the stability of perovskites in humid environments.

In the first stage, we performed structural optimizations of pristine $MAPbI_3$, water-intercalated $MAPbI_3$_H_2O, and monohydrated $MAPbI_3{\cdot}H_2O$. The lattice constant and bandgap of $MAPbI_3$ were calculated to be 6.33 Å and 1.53 eV, which are in good agreement with the experimental values of 6.32−6.33 Å[36,37] and 1.50 eV.[38] For the case of $MAPbI_3$_H_2O, the unit

Received: February 7, 2018
Accepted: April 12, 2018
Published: April 12, 2018

DOI: 10.1021/acs.jpclett.8b00406
J. Phys. Chem. Lett. 2018, 9, 2196−2201

cell containing a water molecule in the large interstitial space formed by the PbI_6 framework became triclinic after optimization. The initial structure of $MAPbI_3{\cdot}H_2O$ with a monoclinic crystalline lattice and experimentally identified atomic positions[39] was also optimized, giving lattice constants of a = 10.46 Å, b = 4.63 Å, c = 11.10 Å, and β = 101.50°, agreeing well with the experimental values.[39] The bandgaps were calculated to be 1.86 eV in $MAPbI_3\_H_2O$ and 2.47 eV in $MAPbI_3{\cdot}H_2O$, being comparable with the previous DFT value of 2.52 eV for the monohydrated phase[19] and experimental measurements.[16]

In the second stage, using the optimized unit cells, we built (3 × 3 × 3) supercells for $MAPbI_3$ (324 atoms) and $MAPbI_3\_H_2O$ (405 atoms) and a (2 × 3 × 2) supercell for $MAPbI_3{\cdot}H_2O$ (360 atoms), with and without vacancy defects, and performed atomic relaxations with fixed lattice constants (see Figures S1−S3). Isolated vacancy point (V_I, V_{MA}, V_{Pb}) and pair defects (V_{MAI}, V_{PbI_2}) were created. For each vacancy defect, various charge states were considered to identify the thermodynamic charge transition levels. Figure 1 presents the defect formation energy diagrams at I-poor (Pb-rich and MA-rich) and I-rich (Pb-poor and MA-poor) conditions. These conditions correspond to an iodine precursor in orthorhombic solid form and a lead precursor in fcc solid form, respectively.

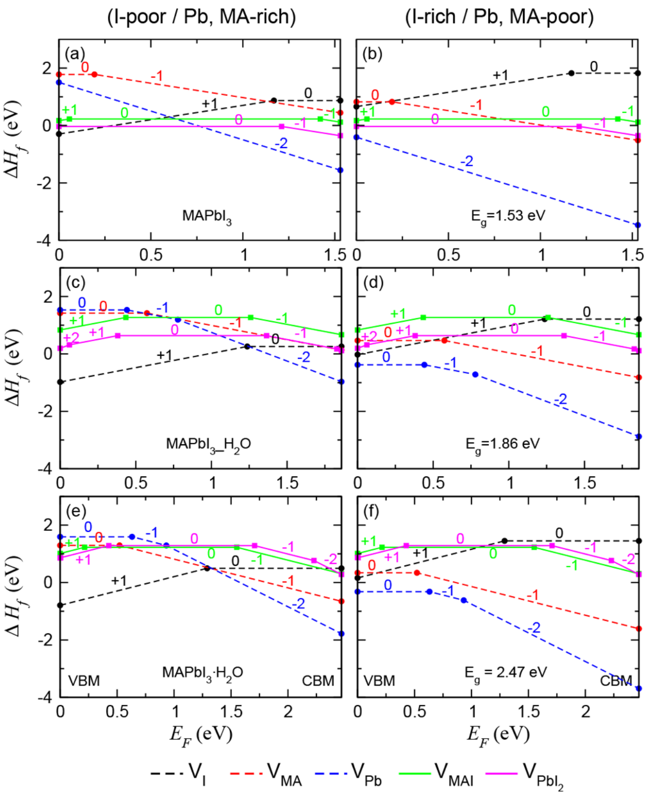

Figure 1. Formation enthalpies of vacancy point and pair defects as a function of the Fermi energy (E_F) under I-poor (Pb-, MA-rich) conditions (left panel) and I-rich (Pb-, MA-poor) conditions (right panel) in (a,b) cubic $MAPbI_3$, (c,d) water-intercalated phase $MAPbI_3\_H_2O$, and (e,f) monohydrate phase $MAPbI_3{\cdot}H_2O$. E_F ranges within the bandgap (E_g) from the valence band maximum (VBM), set to 0 eV, to the conduction band minimum (CBM).

Among the vacancy point defects, lead vacancies with a charge state of −2 (V_{Pb}^{-2}) in these three compounds, along with a −1 charge state (V_{Pb}^{-1}) and neutral state (V_{Pb}^{0}) in the case of hydrous compounds, have the lowest formation energies in the whole range of Fermi energy (E_F) at I-rich conditions. For I-poor growth, meanwhile, the iodine vacancies with a charge state of +1 (V_I^{+1}) have the lowest formation energies in the lower part of E_F, whereas V_{Pb}^{-2} is in the higher range of E_F. Note that for the case of $MAPbI_3$ our results are consistent with previous DFT studies,[31,32] with some minor numerical differences due to the inclusion of dispersion corrections in this work. Under I-poor conditions, MA vacancies with a neutral state (V_{MA}^{0}) and a charge state of −1 (V_{MA}^{-1}) have typically higher formation energies than V_{Pb} and V_I in $MAPbI_3$ and $MAPbI_3\_H_2O$, but in-between values are found in the case of $MAPbI_3{\cdot}H_2O$.

For vacancy pair defects, which can be viewed as compensated partial Schottky-type aggregates, we considered various charge states. We calculated the binding energy defined as $E_b = H_f[A] + H_f[B] - H_f[AB]$.[40] Table 1 summarizes the formation and binding energies of the neutral pairs of V_{MAI}^{0} and $V_{PbI_2}^{0}$ (for E_b of charged pairs, see Table S1). For the case of $MAPbI_3$, the formation energy of V_{MAI}^{0} is 0.23 eV, which is much lower than 1.80 eV reported by Kim et al.[30] If we use the MAI molecule instead of MAI solid as they did, it becomes 1.98 eV, in better agreement. $V_{PbI_2}^{0}$ has a formation energy of −0.03 eV, being slightly lower than 0.03 eV reported by Kim et al.,[30] possibly due to a different crystal lattice. In general, the formation energies of these complex defects in the hydrous compounds are higher than those in pristine $MAPbI_3$.

The formation of $V_{PbI_2}^{0}$ in all of the compounds is more favorable than the formation of the individual vacancy point defects V_I^{+1} and V_{Pb}^{-2} due to their positive binding energies (Table 1). Therefore, it is expected that V_I^{+1} and V_{Pb}^{-2} are formed first (they are dominant defects), and then, the interaction between them leads to the formation of $V_{PbI_2}^{0}$ independently of the hydrous compound. Water adsorption into the perovskite crystal reduces the activation barrier for vacancy-mediated I^- ion migration,[28] resulting in an enhancement of $V_{PbI_2}^{0}$ formation. As shown in Figure 1, the formation energy of V_I^{+1} (V_{Pb}^{-2}) at the I-rich condition is higher (lower) than that at the I-poor condition (their concentrations have a reverse feature), and thus, the reaction rate of $V_{PbI_2}^{0}$ formation can be lower at the I-rich condition (Pb_2^{+} ion migration is quite difficult). Experimentally, I-rich conditions can be realized directly by adding I_3^- in solution.[2] Indirect approaches, such as increasing the PbI_2 concentration relative to MAI,[41] can effectively inhibit the formation of $V_{PbI_2}^{0}$ from the decomposition of $MAPbI_3$. The formation of a passivating $MAPbI_3|PbI_2$ interface ensures a high chemical potential of lead and iodine.[42,43] Surprisingly, the binding energies of V_{MAI}^{0} in the hydrous compounds are negative, although it is positive in the pristine perovskite. This indicates that in the hydrous compounds other products such as HI, CH_3NH_2, and I_2 rather than MAI can be formed during chemical decomposition.

Next, we derived thermodynamic transition levels $\varepsilon(q_1/q_2)$ between defects in different charge states q_1 and q_2. Figure 2 shows the possible transition levels together with the relative band alignment of $MAPbI_3\_H_2O$ and $MAPbI_3{\cdot}H_2O$ with respect to $MAPbI_3$. Water molecules inserted through the film surface extract electrons, resulting in the shift of the valence band maximum (VBM) toward lower values and the conduction band minimum (CBM) toward higher values and thus the bandgap change from the pristine to the water-

DOI: 10.1021/acs.jpclett.8b00406
J. Phys. Chem. Lett. 2018, 9, 2196−2201

Table 1. Formation (H_f) and Binding (E_b) Energies of Schottky-Type Vacancy Pair Defects in $MAPbI_3$, $MAPbI_3\_H_2O$, and $MAPbI_3{\cdot}H_2O$ (unit: eV per defect)

	$MAPbI_3$		$MAPbI_3\_H_2O$		$MAPbI_3{\cdot}H_2O$	
	H_f	E_b	H_f	E_b	H_f	E_b
V^0_{MAI}	0.23	1.45	1.27	−0.25	1.23	−0.21
$V^0_{PbI_2}$	−0.03	0.94	0.64	0.16	1.29	0.28

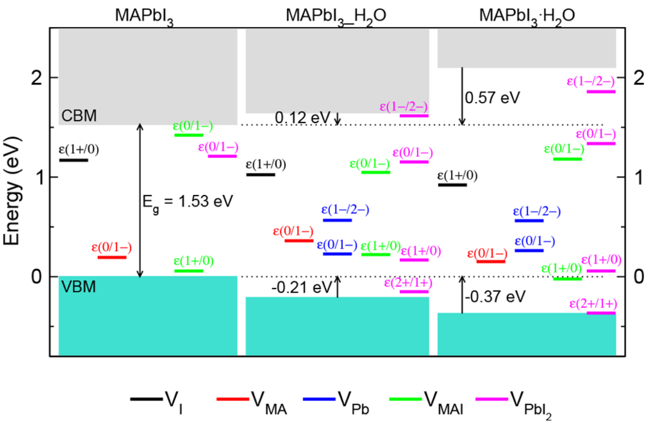

Figure 2. Band alignment and thermodynamic transition levels in $MAPbI_3$, water-intercalated $MAPbI_3\_H_2O$, and monohydrate $MAPbI_3{\cdot}H_2O$, where deep-lying Pb 5d levels are used as a reference for the VBM and CBM of each phase.

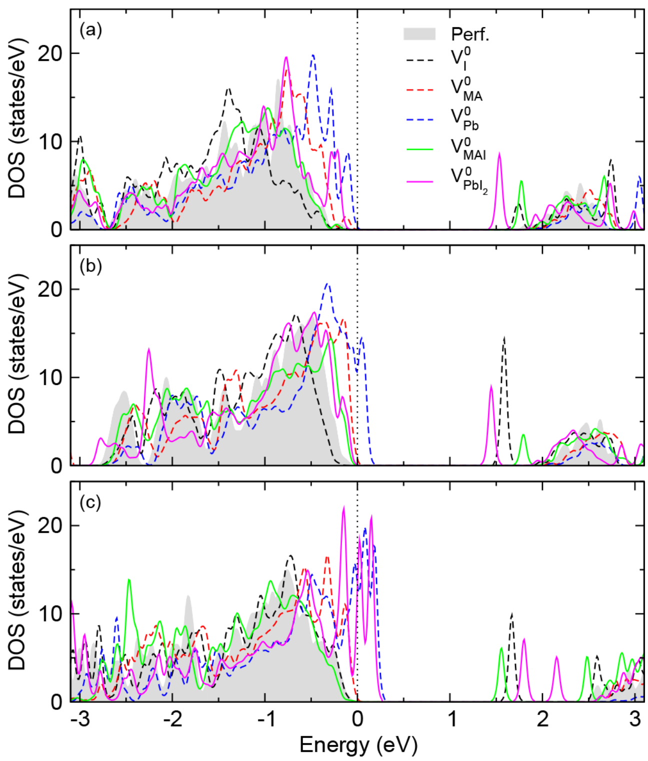

Figure 3. Electronic density of states in perfect and vacancy-containing (a) $MAPbI_3$, (b) water-intercalated phase $MAPbI_3\_H_2O$, and (c) monohydrate phase $MAPbI_3{\cdot}H_2O$. Using semicore 5d levels of Pb far away from the defect as a reference, the VBM in the perfect phase is set to be zero, indicated by the dotted vertical line.

intercalated and to the monohydrated phase. It is apparent that in the case of $MAPbI_3$ all of the vacancy defects have shallow transition levels, whereas in the case of hydrous compounds, the vacancies exhibit deep trap behavior that can facilitate the recombination of charge carriers, resulting in the degradation of solar cell performance. Specifically, in the case of $MAPbI_3$, V_I and V_{MA} are shallow donors and acceptors due to their transition levels $\varepsilon(1+/0)$ and $\varepsilon(0/1-)$ near the CBM and VBM, respectively. In the case of hydrous compounds, transition levels are located deep in the bandgap region, although V_{MA} transition levels are not far away from the valence band. In particular, V_{Pb} has no transition level ($\varepsilon(0/2-)$ inside of the valence band) in $MAPbI_3$, but two deep transition levels $\varepsilon(0/1-)$ and $\varepsilon(1-/2-)$ are possible in the hydrous compounds. Similar features are found for V_{MAI} (two transition levels) and for V_{PbI_2}, which has two/four transition levels in the pristine/hydrous $MAPbI_3$.

The electronic density of states (DOS) in the pristine and vacancy-containing structures is shown in Figure 3. Only the neutral states are considered. To make clear the role of each species, the atom-projected DOS (PDOS) is presented in Figure S4−S6. In all of the compounds, the lower conduction band is from Pb 6p, while the upper valence band is from mostly I 5p states and a minor part from Pb 6s.[44−46] In the case of $MAPbI_3$, V_I formation causes a donor level near the conduction band, and the positive potential results in a downshift of the local valence band, while V_{Pb} and V_{MA} form acceptor states and their negative potential result in a local upshift of the valence band. The DOS characteristics of V_{PbI_2} and V_{MAI} can be explained by combining the effects of individual point defects. Similar features are observed in the hydrous compounds. One distinction is that the n-type donor level created by V_I is deeper in the bandgap due to the presence of the water molecule. The electronic states of the water molecule overlap with I 5p at about −2 (−3) eV and with the MA states at about −4 (−5) eV in $MAPbI_3\_H_2O$ ($MAPbI_3{\cdot}H_2O$) through the hydrogen bonding interaction between water and I atoms of PbI_6 as well as the MA moiety. When the vacancy defect V_I or V_{Pb} is formed, similar interactions are observed.

To study the charge density redistribution during the formation of a vacancy defect, we plot the electron density difference $\Delta\rho = \rho_{V_D} - \rho_{perf} + \rho_D$ in Figure 4. In the case of $MAPbI_3$, charge is depleted around the V_I^+ defect, while charge is accumulated around V_{MA}^- and V_{Pb}^{-2}, as expected. When the hydrous phases are formed, the extent of charge exchange is reduced because the water molecule can donate (for positive point defect) or accept (for negative ones) some electrons, indicating a stabilization by water of the Schottky-type defects. In the absence of water, V_I, V_{MA}, and V_{Pb} with charge states of +1, −1, and −2 are the most stable over a large range of Fermi energy. In the case of hydrous compounds, however, the enhanced polarization due to water opens up alternative charge states, leading to the creation of deep levels, which may enhance nonradiative processes and ultimately lead to the degradation of PSCs. Further research is required to under-

DOI: 10.1021/acs.jpclett.8b00406
J. Phys. Chem. Lett. 2018, 9, 2196−2201

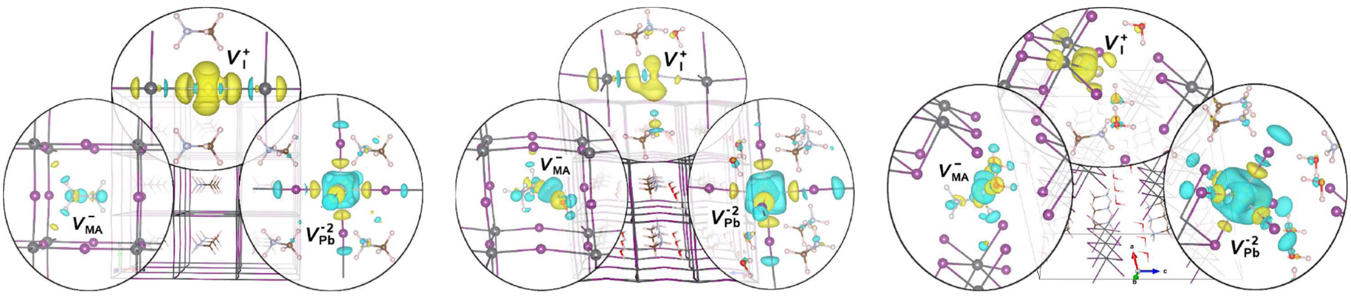

(a) $MAPbI_3$ (b) $MAPbI_3\_H_2O$ (c) $MAPbI_3{\cdot}H_2O$

Figure 4. Isosurface plot of the electronic charge density difference upon formation of vacancy point defects V_I^+, V_{MA}^-, and V_{Pb}^{-2} in (a) $MAPbI_3$, (b) $MAPbI_3\_H_2O$, and (c) $MAPbI_3{\cdot}H_2O$, at a value of 0.0025 $|e|/Å^3$. Yellow (blue) represents the charge depletion (accumulation).

stand the photochemical processes involving these new sub-bandgap electronic states.

In summary, we have investigated defect processes in $MAPbI_3$ and its hydrous phases $MAPbI_3\_H_2O$ and $MAPbI_3{\cdot}H_2O$ in order to reveal the effect of water on the performance and stability of iodide perovskites. The formation of V_{PbI_2} from its individual vacancy point defects is spontaneous, and due to the greatly reduced kinetic barrier for I^- ion migration when hydrated, the concentration of V_I should be reduced to prevent this formation, which can be realized by imposing I-rich conditions. In the hydrous compounds, the formation of individual point defects V_I and V_{MA} is more favorable than the formation of V_{MAI}, and thus, I_2 or CH_3NH_2 or HI can be formed rather than MAI during the decomposition. Unlike in bulk $MAPbI_3$, all of the vacancy defects create deep transition levels in the hydrous compounds arising from electrostatic interactions with water molecules. We note that we have only considered processes involving vacancies, and further pathways may exist, for example, mediated by interstitial defects. To overcome the negative effects of water on the performance and stability of halide perovskites, controlling the processing conditions such as the halide chemical potential during growth and annealing will be important, in addition to the physical encapsulation of devices.

■ COMPUTATIONAL METHODS

The formation enthalpy of a point defect with a charge state q is calculated using the grand canonical expression[40,47,48]

$$\Delta H_f[D^q] \cong \{E[D^q] + E_{corr}[D^q]\} - E_{perf} - n_i\mu_i + qE_F \tag{1}$$

where $E[D^q]$ and E_{perf} are the total energies of the supercell including a defect D and the perfect crystal supercell and n_i and μ_i are the number of removed (minus sign) or added (plus sign) i-type species and its chemical potential. $E_{corr}[D^q]$ is a correction to the error in the total energy of a charged supercell that can be calculated by $E_{corr} = \alpha q^2/\varepsilon L$ in the monopole approximation, where α is the Madelung constant, ε the static dielectric constant, and L the lattice constant.[40,49] Using density functional perturbation theory, we computed the isotropic static dielectric constants to be 23.55, 25.88, and 16.30 for $MAPbI_3$, $MAPbI_3\_H_2O$, and $MAPbI_3{\cdot}H_2O$. E_F is defined with respect to the VBM of the host: $E_F = \epsilon_{VBM} + \Delta\epsilon_F + \Delta V$, where ϵ_{VBM} is the highest occupied eigenvalue, $\Delta\epsilon_F$ is with respect to the VBM, and ΔV is the potential alignment. We have not included a band-filling correction for shallow neutral defects due to its negligible value with large supercell sizes used in this work. Electron self-interaction errors and spin−orbit coupling were not accounted for, which is not expected to affect the comparison between the defect physics of pristine and hydrated $MAPbI_3$ compounds, but they will be important for future work on quantitative computational defect spectroscopy.[50]

The chemical potentials depend on the growth conditions, which can fall between I-rich or I-poor conditions. The I-rich condition corresponds to the iodine precursor in orthorhombic solid form (space group *Cmca*), and thus, the upper limit of the iodine chemical potential is $\mu_I^{rich} = E_{I(orth)}$. The synthesis equations constrain the chemical potentials as follows

$$\mu_{MAI} + \mu_{PbI_2} = \mu_{MAPbI_3} \tag{2}$$

$$\mu_{Pb} + 2\mu_I = \mu_{PbI_2} \tag{3}$$

$$\mu_{MA} + \mu_I = \mu_{MAI} \tag{4}$$

Equations 2 and 3 correspond to the real synthetic reactions, but eq 4 acts only as a theoretical reference. From eq 3, we identified the iodine-poor conditions, $\mu_I^{poor} \approx 1/2(E_{PbI_2} - \mu_{Pb}^{rich})$, where $\mu_{Pb}^{rich} = E_{Pb(fcc)}$ is referred to the bulk Pb in the fcc phase and E_{PbI_2} is referred to the bulk PbI_2 in the rhombohedral phase (space group $P\bar{3}m1$),[46] and the Pb-poor condition, $\mu_{Pb}^{poor} \approx E_{PbI_2} - 2\mu_I^{rich}$. Then, using eqs 2 and 4, the MA-poor and -rich conditions were established like as $\mu_{MA}^{poor} \approx E_{MAPbI_3} - E_{PbI_2} - \mu_I^{rich}$ and $\mu_{MA}^{rich} \approx E_{MAPbI_3} - E_{PbI_2} - \mu_I^{poor}$. For the vacancy pair defects, the chemical potentials were not affected by the iodine chemical potential; $\mu_{MAI} \approx E_{MAPbI_3} - E_{PbI_2}$ and $\mu_{PbI_2} \approx E_{PbI_2}$.

Pseudocubic unit cells were adopted for $MAPbI_3$, and (3 × 3 × 3) and (2 × 3 × 2) supercells were used for vacancy-containing $MAPbI_3$, $MAPbI_3\_H_2O$, and $MAPbI_3{\cdot}H_2O$. The DFT total energies were calculated using the Quantum ESPRESSO code[51] with the ultrasoft pseudopotentials provided in the code and the Perdew−Burke−Ernzerhof (PBE) exchange−correlation functional[52] added by the van der Waals (vdW) energy in the flavor of vdW-DF-OB86.[53] Scalar-relativistic effects are included. A plane-wave cutoff energy of 40 Ry and a Γ point for structural relaxation of vacancy-containing supercells and 2 × 2 × 2 special k-points for DOS calculations were used for all of the configurations. All of the atomic positions of each configuration were relaxed until the forces on the atoms converged to 5×10^{-5} Ry/Bohr.

■ ASSOCIATED CONTENT

Ⓢ Supporting Information

The Supporting Information is available free of charge on the ACS Publications website at DOI: 10.1021/acs.jpclett.8b00406.

DOI: 10.1021/acs.jpclett.8b00406
J. Phys. Chem. Lett. 2018, 9, 2196−2201

Optimized atomistic structures of perfect and vacancy-containing supercells, binding energies of vacancy pair defects with various charge states, and projected density of states (PDF)

AUTHOR INFORMATION

Corresponding Authors

*E-mail: ryongnam14@yahoo.com (C.-J.Y.).
*E-mail: a.walsh@imperial.ac.uk (A.W.).

ORCID

Chol-Jun Yu: 0000-0001-9523-4325
Aron Walsh: 0000-0001-5460-7033

Notes

The authors declare no competing financial interest.

ACKNOWLEDGMENTS

This work is supported as part of the fundamental research project "Design of Innovative Functional Materials for Energy and Environmental Application" (No. 2016-20) funded by the State Committee of Science and Technology, DPR Korea. Computations were performed on the HP Blade System C7000 (HP BL460c) that is owned by the Faculty of Materials Science, Kim Il Sung University. A.W. is supported by a Royal Society University Research Fellowship and EPSRC Grant No. EP/K016288/1.

REFERENCES

(1) Kojima, A.; Teshima, K.; Shirai, Y.; Miyasaka, T. Organometal Halide Perovskites as Visible-Light Sensitizers for Photovoltaic Cells. *J. Am. Chem. Soc.* **2009**, *131*, 6050−6051.

(2) Yang, W. S.; et al. Iodide Management in Formamidinium-Lead-Halide-Based Perovskite Layers for Efficient Solar Cells. *Science* **2017**, *356*, 1376−1379.

(3) Wang, D.; Wright, M.; Elumalai, N. K.; Uddin, A. Stability of Perovskite Solar Cells. *Sol. Energy Mater. Sol. Cells* **2016**, *147*, 255−275.

(4) Berhe, T. A.; Su, W.-N.; Chen, C.-H.; Pan, C.-J.; Cheng, J.-H.; Chen, H.-M.; Tsai, M.-C.; Chen, L.-Y.; Dubale, A. A.; Hwang, B.-J. Organometal Halide Perovskite Solar Cells: Degradation and Stability. *Energy Environ. Sci.* **2016**, *9*, 323−356.

(5) Li, B.; Li, Y.; Zheng, C.; Gao, D.; Huang, W. Advancements in the Stability of Perovskite Solar Cells: Degradation Mechanisms and Improvement Approaches. *RSC Adv.* **2016**, *6*, 38079−38091.

(6) Manser, J. S.; Saidaminov, M. I.; Christians, J. A.; Bakr, O. M.; Kamat, P. V. Making and Breaking of Lead Halide Perovskites. *Acc. Chem. Res.* **2016**, *49*, 330−338.

(7) Huang, W.; Manser, J. S.; Kamat, P. V.; Ptasinska, S. Evolution of Chemical Composition, Morphology, and Photovoltaic Efficiency of $CH_3NH_3PbI_3$ Perovskite under Ambient Conditions. *Chem. Mater.* **2016**, *28*, 303−311.

(8) Huang, J.; Tan, S.; Lund, P. D.; Zhou, H. Impact of H_2O on Organic-inorganic Hybrid Perovskite Solar Cells. *Energy Environ. Sci.* **2017**, *10*, 2284−2311.

(9) You, J.; et al. Improved air stability of perovskite solar cells via solution-processed metal oxide transport layers. *Nat. Nanotechnol.* **2015**, *11*, 75−81.

(10) Niu, G. D.; Li, W. Z.; Meng, F. Q.; Wang, L. D.; Dong, H. P.; Qiu, Y. Study on the Stability of $CH_3NH_3PbI_3$ Films and the Effect of Post-Modification by Aluminum Oxide in All-Solid-State Hybrid Solar Cells. *J. Mater. Chem. A* **2014**, *2*, 705−710.

(11) Niu, G. D.; Guo, X. D.; Wang, L. D. Review of Recent Progress in Chemical Stability of Perovskite Solar Cells. *J. Mater. Chem. A* **2015**, *3*, 8970−8980.

(12) Frost, J. M.; Butler, K. T.; Brivio, F.; Hendon, C. H.; van Schilfgaarde, M.; Walsh, A. Atomistic Origins of High-Performance in Hybrid Halide Perovskite Solar Cells. *Nano Lett.* **2014**, *14*, 2584−2590.

(13) Zhao, J.; et al. Investigation of the Hydrolysis of Perovskite Organometallic Halide $CH_3NH_3PbI_3$ in Humidity Environment. *Sci. Rep.* **2016**, *6*, 21976.

(14) Yang, J.; Siempelkamp, B. D.; Liu, D.; Kelly, T. L. Investigation of $CH_3NH_3PbI_3$ Degradation Rates and Mechanisms in Controlled Humidity Environments Using in Situ Techniques. *ACS Nano* **2015**, *9*, 1955−1963.

(15) Christians, J. A.; Miranda Herrera, P. A.; Kamat, P. V. Transformation of the Excited State and Photovoltaic Efficiency of $CH_3NH_3PbI_3$ Perovskite upon Controlled Exposure to Humidified Air. *J. Am. Chem. Soc.* **2015**, *137*, 1530−1538.

(16) Leguy, A. M. A.; et al. Reversible Hydration of $CH_3NH_3PbI_3$ in Films, Single Crystals, and Solar Cells. *Chem. Mater.* **2015**, *27*, 3397−3407.

(17) Hao, F.; Stoumpos, C. C.; Liu, Z.; Chang, R. P. H.; Kanatzidis, M. G. Controllable Perovskite Crystallization at a Gas-Solid Interface for Hole Conductor-Free Solar Cells with Steady Power Conversion Efficiency over 10%. *J. Am. Chem. Soc.* **2014**, *136*, 16411−16419.

(18) Song, Z.; Abate, A.; Watthage, S. C.; Liyanage, G. K.; Phillips, A. B.; Steiner, U.; Graetzel, M.; Heben, M. J. Perovskite Solar Cell Stability in Humid Air: Partially Reversible Phase Transitions in the PbI_2-CH_3NH_3I-H_2O System. *Adv. Energy Mater.* **2016**, *6*, 1600846.

(19) Shirayama, M.; Kato, M.; Miyadera, T.; Sugita, T.; Fujiseki, T.; Hara, S.; Kadowaki, H.; Murata, D.; Chikamatsu, M.; Fujiwara, H. Degradation Mechanism of $CH_3NH_3PbI_3$ Perovskite Materials upon Exposure to Humid Air. *J. Appl. Phys.* **2016**, *119*, 115501.

(20) Ahn, N.; Jeon, I.; Yoon, J.; Kauppinen, E. I.; Matsuo, Y.; Maruyama, S.; Choi, M. Carbon-sandwiched Perovskite Solar Cell. *J. Mater. Chem. A* **2018**, *6*, 1382.

(21) Jeon, I.; Ueno, H.; Seo, S.; Aitola, K.; Nishikubo, R.; Saeki, A.; Okada, H.; Boschloo, G.; Maruyama, S.; Matsuo, Y. Lithium-Ion Endonhedral Fullerene (Li^+C_{60}) Dopants in Stable Perovskite Solar Cells Induce Anti-oxidation. *Angew. Chem., Int. Ed.* **2018**, DOI: 10.1002/anie.201800816.

(22) Zhang, L.; Sit, P. H.-L. Ab Initio Study of Interaction of Water, Hydroxyl Radicals, and Hydroxide Ions with $CH_3NH_3PbI_3$ and $CH_3NH_3PbBr_3$ Surfaces. *J. Phys. Chem. C* **2015**, *119*, 22370−22378.

(23) Quarti, C.; Grancini, G.; Mosconi, E.; Bruno, P.; Ball, J. M.; Lee, N. M.; Snaith, H. J.; Petrozza, A.; De Angelis, F. The Raman Spectrum of the $CH_3NH_3PbI_3$ Hybrid Perovskite: Interplay of Theory and Experiment. *J. Phys. Chem. Lett.* **2014**, *5*, 279−284.

(24) Gottesman, R.; Haltzi, E.; Gouda, L.; Tirosh, S.; Bouhadana, Y.; Zaban, A.; Mosconi, E.; de Angelis, F. Extremely Slow Photoconductivity Response of $CH_3NH_3PbI_3$ Perovskites Suggesting Structural Changes under Working Conditions. *J. Phys. Chem. Lett.* **2014**, *5*, 2662−2669.

(25) Eames, C.; Frost, J. M.; Barnes, P. R. F.; O'Regan, B. C.; Walsh, A.; Islam, M. S. Ionic Transport in Hybrid Lead Iodide Perovskite Solar Cells. *Nat. Commun.* **2015**, *6*, 7497.

(26) Haruyama, J.; Sodeyama, K.; Han, L.; Tateyama, Y. First-Principles Study of Ion Diffusion in Perovskite Solar Cell Sensitizers. *J. Am. Chem. Soc.* **2015**, *137*, 10048−10051.

(27) Azpiroz, J. M.; Mosconi, E.; Bisquert, J.; De Angelis, F. Defects Migration in Methylammonium Lead Iodide and their Role in Perovskite Solar Cells Operation. *Energy Environ. Sci.* **2015**, *8*, 2118−2127.

(28) Jong, U.-G.; Yu, C.-J.; Ri, G.-C.; McMahon, A. P.; Harrison, N. M.; Barnes, P. R. F.; Walsh, A. Influence of Water Intercalation and Hydration on Chemical Decomposition and Ion Transport in Methylammonium Lead Halide Perovskites. *J. Mater. Chem. A* **2018**, *6*, 1067−1074.

(29) Walsh, A.; Scanlon, D. O.; Chen, S.; Gong, X. G.; Wei, S.-H. Self-regulation Mechanism for Charged Point Defects in Hybrid Halide Perovskites. *Angew. Chem., Int. Ed.* **2015**, *54*, 1791−1794.

(30) Kim, J.; Lee, S.-H.; Lee, J. H.; Hong, K.-H. The Role of Intrinsic Defects in Methylammonium Lead Iodide Perovskite. *J. Phys. Chem. Lett.* **2014**, *5*, 1312−1317.

DOI: 10.1021/acs.jpclett.8b00406
J. Phys. Chem. Lett. 2018, 9, 2196−2201

(31) Buin, A.; Comin, R.; Xu, J.; Ip, A. H.; Sargent, E. H. Halide-Dependent Electronic Structure of Organolead Perovskite Materials. *Chem. Mater.* **2015**, *27*, 4405−4412.
(32) Yin, W.-J.; Shi, T.; Yan, Y. Unusual Defect Physics in $CH_3NH_3PbI_3$ Perovskite Solar Cell Absorber. *Appl. Phys. Lett.* **2014**, *104*, 063903.
(33) Du, M. H. Efficient Carrier Transport in Halide Perovskites: Theoretical Perspectives. *J. Mater. Chem. A* **2014**, *2*, 9091−9098.
(34) Koocher, N. Z.; Saldana-Greco, D.; Wang, F.; Liu, S.; Rappe, A. M. Polarization Dependence of Water Adsorption to $CH_3NH_3PbI_3$ (001) Surfaces. *J. Phys. Chem. Lett.* **2015**, *6*, 4371−4378.
(35) Tong, C.-J.; Geng, W.; Tang, Z.-K.; Yam, C.-Y.; Fan, X.-L.; Liu, J.; Lau, W.-M.; Liu, L.-M. Uncovering the Veil of the Degradation in Perovskite $CH_3NH_3PbI_3$ upon Humidity Exposure: A First-Principles Study. *J. Phys. Chem. Lett.* **2015**, *6*, 3289−3295.
(36) Poglitsch, A.; Weber, D. Dynamic Disorder in Methylammoniumtrihalogenoplumbates (ii) Observed by Millimeter-wave Spectroscopy. *J. Chem. Phys.* **1987**, *87*, 6373−6378.
(37) Weller, M. T.; Weber, O. J.; Henry, P. F.; Di Pumpo, A. M.; Hansen, T. C. Complete Structure and Cation Orientation in the Perovskite Photovoltaic Methylammonium Lead Iodide between 100 and 352 K. *Chem. Commun.* **2015**, *51*, 4180−4183.
(38) Kim, H. S.; et al. Lead Iodide Perovskite Sensitized All-Solid-State Submicron Thin Film Mesoscopic Solar Cell with Efficiency Exceeding 9%. *Sci. Rep.* **2012**, *2*, 591.
(39) Imler, G. H.; Li, X.; Xu, B.; Dobereiner, G. E.; Dai, H.-L.; Rao, Y.; Wayland, B. B. Solid State Transformation of the Crystalline Monohydrate $(CH_3NH_3)PbI_3(H_2O)$ to the $(CH_3NH_3)PbI_3$ Perovskite. *Chem. Commun.* **2015**, *51*, 11290−11292.
(40) Freysoldt, C.; Grabowski, B.; Hickel, T.; Neugebauer, J.; Kresse, G.; Janotti, A.; Van de Walle, C. G. First-principles Calculations for Point Defects in Solids. *Rev. Mod. Phys.* **2014**, *86*, 253−305.
(41) Ko, H.-S.; Lee, J. W.; Park, N.-G. 15.76% Efficiency Perovskite Solar Cells Prepared under High Relative Humidity; Importance of PbI_2 Morphology in Two-step Deposition of $CH_3NH_3PbI_3$. *J. Mater. Chem. A* **2015**, *3*, 8808−8815.
(42) Supasai, T.; et al. Formation of a Passivating $CH_3NH_3PbI_3/PbI_2$ Interface during Moderate Heating of $CH_3NH_3PbI_3$ Layers. *Appl. Phys. Lett.* **2013**, *103*, 183906.
(43) Wang, L.; et al. Femtosecond Time-Resolved Transient Absorption Spectroscopy of $CH_3NH_3PbI_3$ Perovskite Films: Evidence for Passivation Effect of PbI_2. *J. Am. Chem. Soc.* **2014**, *136*, 12205−12208.
(44) Yu, C.-J.; Jong, U.-G.; Ri, M.-H.; Ri, G.-C.; Pae, Y.-H. Electronic Structure and Photoabsorption Property of Pseudo-cubic Perovskites $CH_3NH_3PbX_3$ (X = I, Br) including van der Waals Interaction. *J. Mater. Sci.* **2016**, *51*, 9849−9854.
(45) Jong, U.-G.; Yu, C.-J.; Ri, J.-S.; Kim, N.-H.; Ri, G.-C. Influence of Halide Composition on the Structural, Electronic, and Optical Properties of Mixed $CH_3NH_3Pb(I_{1-x}Br_x)_3$ Perovskites Calculated using the Virtual Crystal Approximation Method. *Phys. Rev. B: Condens. Matter Mater. Phys.* **2016**, *94*, 125139.
(46) Jong, U.-G.; Yu, C.-J.; Jang, Y.-M.; Ri, G.-C.; Hong, S.-N.; Pae, Y.-H. Revealing the Stability and Efficiency Enhancement in Mixed-halide Perovskites $MAPb(I_{1-x}Cl_x)_3$ with ab initio calculations. *J. Power Sources* **2017**, *350*, 65−72.
(47) Zhang, S. B.; Northrup, J. E. Chemical Potential Dependence of Defect Formation Energies in GaAs: Application to Ga Self-Diffusion. *Phys. Rev. Lett.* **1991**, *67*, 2339.
(48) Kumagai, Y.; Oba, F. Electrostatics-based Finite-size corrections for First-principles Point Defect Calculations. *Phys. Rev. B: Condens. Matter Mater. Phys.* **2014**, *89*, 195205.
(49) Makov, G.; Payne, M. C. Periodic Boundary Conditions in Ab Initio Calculations. *Phys. Rev. B: Condens. Matter Mater. Phys.* **1995**, *51*, 4014.
(50) Du, M. H. Density Functional Calculations of Native Defects in $CH_3NH_3PbI_3$: Effects of Spin-Orbit Coupling and Self-Interaction Error. *J. Phys. Chem. Lett.* **2015**, *6*, 1461−1466.
(51) Giannozzi, P.; Baroni, S.; Bonini, N.; Calandra, M.; Car, R.; et al. QUANTUM ESPRESSO: a Modular and Open-source Software Project for Quantum Simulations of Materials. *J. Phys.: Condens. Matter* **2009**, *21*, 395502.
(52) Perdew, J. P.; Burke, K.; Ernzerhof, M. Generalized Gradient Approximation Made Simple. *Phys. Rev. Lett.* **1996**, *77*, 3865.
(53) Klimeš, J.; Bowler, D. R.; Michaelides, A. Van der Waals Density Functionals Applied to Solids. *Phys. Rev. B: Condens. Matter Mater. Phys.* **2011**, *83*, 195131.

DOI: 10.1021/acs.jpclett.8b00406
J. Phys. Chem. Lett. 2018, 9, 2196−2201